Mechanically Induced Chromatin Condensation Requires Cellular Contractility in Mesenchymal Stem Cells

Su-Jin Heo[1,2], Woojin M. Han[2], Spencer E. Szczesny[1,3], Brian D. Cosgrove[1,2,3], Dawn M. Elliott[4], David A. Lee[6], Randall L. Duncan[4,5], and Robert L. Mauck[1,2,3]*

[1]McKay Orthopaedic Research Laboratory, Department of Orthopaedic Surgery, Perelman School of Medicine, University of Pennsylvania, Philadelphia, PA, USA

[2]Department of Bioengineering, School of Engineering and Applied Science, University of Pennsylvania, Philadelphia, PA, USA

[3]Translational Musculoskeletal Research Center, Philadelphia VA Medical Center, Philadelphia, PA, USA

[4]Department of Biomedical Engineering, University of Delaware, Newark, DE, USA

[5]Department of Biological Sciences, University of Delaware, Newark, DE, USA

[6]Institute of Bioengineering, School of Engineering and Materials Science, Queen Mary University of London, London, UK

***Address for Correspondence**:
Robert L. Mauck, Ph.D.
Mary Black Ralston Professor of Orthopaedic Surgery
Professor of Bioengineering

McKay Orthopaedic Research Laboratory
Department of Orthopaedic Surgery
Perelman School of Medicine
University of Pennsylvania
36th Street and Hamilton Walk
Philadelphia, PA 19104
Phone: (215) 898-3294
Fax: (215) 573-2133
Email: lemauck@mail.med.upenn.edu

Short Title: Contractility and Chromatin Condensation

Keywords: Stem cells, Chromatin condensation, Mechanotransduction, Purinergic signaling, TGF-β superfamily, Cellular contractility

ABSTRACT

Mechanical cues play important roles in directing the lineage commitment of mesenchymal stem cells (MSCs). In this study, we explored the molecular mechanisms by which dynamic tensile loading (DL) regulates chromatin organization in this cell type. Our previous findings indicated that the application of DL elicited a rapid increase in chromatin condensation through purinergic signaling mediated by adenosine triphosphate (ATP). Here, we show that the rate and degree of condensation depends on the frequency and duration of mechanical loading, and that ATP release requires acto-myosin based cellular contractility. Increases in baseline cellular contractility via the addition of an activator of G-protein coupled receptors (lysophosphatidic acid) induced rapid ATP release, resulting in chromatin condensation independent of loading. Conversely, inhibition of contractility through pretreatment with either a RhoA/Rock inhibitor (Y27632) or MLCK inhibitor (ML7) abrogated ATP release in response to DL, blocking load-induced chromatin condensation. With loading, ATP release occurred very rapidly (within the first 10-20 seconds), while changes in chromatin occurred at a later time point (~10 minutes), suggesting a downstream biochemical pathway mediating this process. When cells were pre-treated with blockers of the TGF superfamily, purinergic signaling in response to DL was also eliminated. Further analysis showed that this pretreatment decreased contractility, implicating activity in the TGF pathway in the establishment of the baseline contractile state of MSCs (in the absence of exogenous ligands). These data indicate that chromatin condensation in response to DL is regulated through the interplay between purinergic and RhoA/Rock signaling, and that ligand-less activity in the TGF/BMP signaling pathway contributes to the establishment of baseline contractility in MSCs.

INTRODUCTION

Mesenchymal stem cells (MSCs) isolated from bone marrow are capable of differentiating along multiple lineages, including adipocytes, osteocytes, and chondrocytes, when they are exposed to soluble differentiation factors (1-3). Each cell phenotype is characterized by changes in gene expression, which is accompanied by chromatin remodeling and changes in epigenetic markers (4). That is, as stem cells adopt a specific lineage, the chromatin within their nuclei condenses into heterochromatin through histone or DNA modification (e.g., methylation and acetylation) (5-7), which leads to gene suppression in the condensed regions and reduction in stem cell pluripotency (8, 9). Other lineage specific genes located within small, non-condensed euchromatic regions retain expression at high levels (10, 11). In addition to soluble factors, recent studies demonstrate that exogenous mechanical cues play an important role in determining stem cell fate and driving changes in the epigenetic state (12, 13). However, little is known regarding how exogenous mechanical forces guide MSC lineage specification and regulate genome architecture to induce and maintain the differentiated phenotype.

A number of histological methods exist to visualize markers of chromatin modification and condensation, most commonly, the detection of methylated histone residues (i.e., H3K27me3). More recently, Irianto et al. developed an image analysis algorithm based on detectable edges in DAPI stained nuclei to quantify the degree to which chromatin is condensed (14, 15). This image analysis method provides a validated, unbiased, and quantitative measure termed the chromatin condensation parameter (CCP). This method was initially validated via osmotic challenge chondrocytes (which increases chromatin condensation) with condensation confirmed by transmission electron microscopy of the cell nuclei (14). We have likewise shown that the CCP measure can detect changes in response to small molecule modifiers of chromatin condensation (e.g. GSK343, an EZH2 inhibitor which blocks the trimethylation of H3K27 and Trichostatin A, an HDAC inhibitor that decondenses the chromatin) (16). While measures of CCP do not identify specific epigenetic modifications, and do not provide an absolute

measure of condensation, this measure does enable rapid comparisons between experimental groups related to changes in the organization and density of the genetic material.

Acto-myosin based cellular contractility likely mediates mechanically-driven changes in stem cell fate since it is essential for cellular mechanotransduction of physical signals (17-20). Indeed, studies from our lab and others have shown that acto-myosin based cellular contractility modulates stem cell differentiation and chromatin remodeling (16, 21, 22). Specifically, we showed that active cell contractility was necessary to induce chromatin condensation within MSCs in response to dynamic mechanical loading (16). Furthermore, we demonstrated that such dynamic loading (DL)-induced chromatin condensation in MSCs required ATP release through hemichannels and subsequent calcium signaling (16). In addition, since ATP is stored in intracellular vesicles and discharged through fusion with the cell membrane (23), ATP release in response to mechanical loading likely occurs in bursts with necessary refractory periods to refill the intracellular stores. It is unclear how such bursts in ATP signaling compares to the time course of mechanical loading (i.e., frequency and duration) as well as of chromatin condensation. Furthermore, ATP-dependent purinergic signaling is closely associated with actin stress fiber formation and changes in cellular contractility (23). This suggests that ATP signaling may not be solely downstream of mechanical signaling but may also reinforce cytoskeletal tension, thereby priming cells for further mechanical stimulation. Finally, gene expression levels of transforming growth factor beta (TGF-β), which is a potent mediator of stem cell differentiation (24-26), also increase with DL (16) and may additionally regulate chromatin remodeling. Despite our growing understanding of the effects of exogenous mechanical forces on MSC behavior, the mechanisms by which mechanically-induced signaling pathways and cellular contractility interact to regulate chromatin remodeling and MSC fate remain poorly understood.

The objective of this study was to identify how chromatin remodeling within MSCs is influenced by the timing of applied dynamic loading and ATP signaling, and how both ATP and TGF-β interact with cellular contractility to mediate the mechanically-driven MSC response. Specifically, we investigated the

effect of loading frequency and duration on chromatin condensation and probed the importance of cellular contractility on this process. In addition, we determined the timing of ATP release during loading and investigated the interplay between ATP signaling and acto-myosin contractility. Finally, we examined whether these changes were, in part, mediated through the TGF-β signaling pathway and delineated the manner by which these pathways interact with mechanically induced purinergic signaling. Our findings enhance our understanding of how mechanical stimulation induces long-term changes in MSC phenotype via epigenetic modification, which is vital for its successful use in tissue engineering applications.

MATERIALS AND METHODS

Preparation of aligned nanofibrous scaffolds and MSC culture on scaffolds

To fabricate aligned poly(ε-caprolactone) (PCL) scaffolds, a PCL solution (14.3% wt/vol in 1:1 tetrahydrofuran and N,N-dimethylformamide) was loaded into a syringe (20 ml) and extruded at a rate of 2.5 ml/hour through a stainless steel needle (18G, charged to +13 kV) (27). To direct fiber alignment, PCL fibers were collected onto a cylindrical mandrel rotating with a surface velocity of 10 m/sec. PCL scaffolds were hydrated and sterilized in ethanol (100, 70, 50, 30%; 30 minutes/step), and incubated in a fibronectin solution (20 μg/ml) overnight to enhance cell attachment (27, 28).

Mesenchymal stem cells were isolated from juvenile bovine tibiofemoral joints (3-6 months old, Research 87, Inc., Boylston, MA) as in (29) and 2×10^5 cells were seeded onto each side of the scaffold ($60 \times 5 \times \sim0.5$ mm^3). Scaffolds were cultured in a chemically defined serum free medium (CM) (high glucose DMEM with 1× penicillin/streptomycin/fungizone (PSF), 0.1 μM dexamethasone, 50 μg/ml ascorbate 2-phosphate, 40 μg/ml L-proline, 100 μg/ml sodium pyruvate, 6.25 μg/ml insulin, 6.25 μg/ml transferrin, 6.25 ng/ml selenous acid, 1.25 mg/ml bovine serum albumin and 5.35 μg/ml linoleic acid) without any additional growth factors (29).

Dynamic mechanical perturbation of MSC-seeded scaffolds

To apply dynamic tensile loading (DL), MSC seeded scaffolds were placed into a custom tensile loading bioreactor (12). DL was applied in CM (without any additional growth factors, strain: 3 %, sinusoidal cyclic loading) at varying frequencies (0.2 ~ 2 Hz) for varying durations (up to 600 sec), following 2 days of pre-culture in CM. To investigate the effect of acto-myosin contractility, constructs were pre-treated with either the myosin light chain kinase inhibitor ML7 (25 μM, for 1 h, Tocris Biosciences) or the Rho kinase inhibitor, Y27632 (Y27, 10 μM, for 1 h, EMD Millipore, Bedford, MA) to decrease contractility (22). Lysophosphatidic acid (50 μM, LPA, 15 min, Sigma) activates RhoA GTPase through binding to its receptor and was used to transiently increase contractility prior to mechanical stimulation (22).

Determination of the chromatin condensation parameter (CCP)

To assess chromatin condensation, an image analysis method was adapted from a previous approach described by Irianto et al. (14, 15). Briefly the constructs were fixed in 4% paraformaldehyde for 30 mins at 37°C. A permeabilization solution (0.1% Triton X-100 in PBS supplemented with 320 mM sucrose and 6 mM magnesium chloride) was added followed by three washes in PBS. Nuclei were stained with DAPI (ProLong® Gold anti-fade reagent with DAPI, P36935, Molecular Probes®, Grand Island, NY) and scanned across their mid-section using a confocal microscope (Zeiss, LSM 510, Jena, Germany). To calculate the chromatin condensation parameter (CCP), a gradient-based Sobel edge detection algorithm was employed to produce an edge map (14, 15), a thinning morphological algorithm was then used to reduce strong edge lines into single-pixel-thickness entities using MATLAB. After the border edge of the nucleus was excluded, the area of edges was measured. To compute the CCP, this value was divided by the cross-sectional area of the nucleus (14, 15). This image analysis method can be utilized to quantify changes in chromatin architecture in fluorescently labelled nuclei.

Measurements of extracellular ATP and intracellular Ca^{2+}

To measure the concentration of ATP in conditioned media, a commercial luciferin/luciferase based ATP Assay Kit was used (KA1661, Abnova, Taipei City, Taiwan), according to manufacturer's instructions. Briefly, 10 µl of conditioned media was transferred into a white opaque 96 well plate. 96 µl of Assay Buffer with 1 µl Substrate and 1 µl ATP Enzyme was then added to each well. Readings were taken using a luminescence probe with all emission wavelengths on Synergy™ 2 (BioTek® Instruments Inc., Winooski, VT).

To determine changes in intracellular Ca^{2+} concentration ($[Ca^{2+}]_i$), MSCs were loaded with the fluorescent calcium indicator Cal-520™ AM (15 µM, AAT Bioquest, Sunnyvale, CA) for 1 h at 37 °C. Scaffolds were placed in a custom micro-tensile device (30), and preloaded to 30 mN prior to taking images. Images were obtained using a confocal microscope (LSM 5 LIVE; Carl Zeiss, Jena, Germany) every 4 s for 10 min (0.25 Hz scanning frequency) (30-32). To investigate the effect of mechanical perturbation on changes in intracellular $[Ca^{2+}]_i$, grip-to-grip strains of 0 and 3 % were applied at 0.05 %/sec (n = 3 samples), and a time-series of images of $[Ca^{2+}]_i$ in individual cells was recorded for an additional 10 min after the cessation of loading. A custom MATLAB (The Mathworks Inc., Natick, MA, USA) program was used to analyze $[Ca^{2+}]_i$ oscillations (% responding cells and the number of peaks in ten minutes, **sFig. 5**) as in (30).

Assessment of ATP release and intracellular visualization

Given that DL caused rapid ATP release by MSCs, we next investigated the timing over which this occurred. For this, MSC seeded scaffolds were subjected to 4 different DL conditions (3%, 0.2 Hz for 30 sec, 1 Hz for 30 sec, 0.2 Hz for 600 sec, 1 Hz for 600 sec), and ATP concentration was measured in the media after the cessation of loading. Other constructs were subjected to DL for 30s at 0.2 Hz or 1 Hz followed by free swelling culture for a total 600 sec. In other sets, constructs were subjected to DL for 30s at 0.2 Hz or 1 Hz, and, after cessation of DL, the conditioned media was switched to fresh media. These

constructs were cultured in this new media up to 600s. As additional controls, scaffolds were cultured under free swelling (FS) conditions in CM for 600s or were switched to new CM at 30s followed by culture up to 600 seconds. In another control group, DL was applied at 1Hz up to 600s, with the media changed to fresh CM at 30s. These groups are outlined schematically in **Fig. 2B**. ATP concentration in each conditioned media and CCP was measured in each of these conditions at 600 seconds, as described above.

Next, to investigate how fast ATP was released in the context of loading, we applied DL (3%, 1Hz) for periods of time ranging from 5s to 30 s and collected the DL conditioned medium. These scaffolds were then cultured in fresh CM for an additional 600s and ATP was measured in these media as well. To visualize the intracellular localization of ATP, cells on scaffolds were stained with quinacrine dihydrochloride (QD, 5 μM, Q3251, Sigma). QD staining has previously been reported to identify ATP filled vesicles in a number of different cell types (33). For this experiment, MSC-seeded scaffolds were labeled with QD in CM for 1h. After 30 s of DL (1 Hz, 3%) or free swelling culture, constructs were fixed in 4% paraformaldehyde for 30 mins at 37°C, and visualized using a confocal microscope (Zeiss, LSM 510, Jena, Germany). The mean intensity of QD staining in the cytoplasm was measured using Image J.

To determine how quickly ATP stores could be replenished, DL (1Hz, 3%, 30s) was applied at several time points after the initial loading event, and ATP concentration in the DL conditioned media was measured. Restoration of ATP-filled vesicles was also visualized via QD staining. In addition, to inhibit F1F0 in mitochondria (blocking H+ transport coupled to ATP synthesis) (34-36), another set of constructs was treated with oligomycin (Oligo, 10 μg/ml, 75351, Sigma) or dicyclohexylcarbodiimide (DCC, 100 μM, D80002, Sigma) after the cessation of DL (1Hz, 3%, 30s), and QC labeling of ATP filled vesicles was again monitored.

Pharmacologic blockade of TGF-β signaling

To determine the role of TGF-β signaling in load induced chromatin condensation and ATP release, MSC-seeded constructs were pre-treated with SB431542 (SB, 10 μM, Sigma) to inhibit Smad 2/3 (TGFβ) signaling or LDN193189 (LDN, 100 nM, Reagents Direct) to inhibit Smad 1/5/8 (BMP) signaling. Constructs were pre-treated with these inhibitors for 2 hours prior to application of DL (1 Hz, 3%, 600 sec). Afterwards, constructs were fixed and CCP quantified as described above. In addition, the DL-conditioned media was collected to measure ATP concentration. In another experiment, exogenous ATP was added (for 30 minutes) to MSCs that had been pre-treated with these inhibitors, followed by quantification of CCP. Similarly, changes in intracellular Ca^{2+} after pre-treatment with SB or LDN was investigated as described above, immediately following the application of 0 or 3% strain (n = 3 samples).

Traction force microscopy (TFM)

For traction force experiments, MSCs were seeded onto polyacrylamide (PA) hydrogels (Young's Modulus, E = 10 kPa, 3000 cells/cm^2, prepared on glass slides) and allowed to attach for 24 hrs before carrying out TFM (22). Cells and embedded beads (0.2-μm-diameter fluorescent microspheres, F8810, Invitrogen, Carlsbad, CA) were imaged using a Deltavision Deconvolution Microscope and all imaging was performed in an environmental chamber (37°C, 5% CO_2). TFM data analysis (stack alignment, PIV, and FTTC) was carried out using an FTTC plugin in Image J and a custom MATLAB script as in (22, 37). In some studies, cells were treated with Y27632 (Y27, 10 μM. for 1 hour, Calbiochem Merck), SB431542 (SB, 10 μM, for 2 hours, Sigma), or LDN193189 (LDN, 100 nM, for 2 hours, Reagents Direct) prior to measurement of traction forces. In additional studies, a neutralizing antibody to TGF-β (1μg/ml, MAB1835, R&D Systems) was included for 1 hour at 37 °C prior to measurement of traction forces.

Statistical analyses

Statistical analysis was performed using ANOVA with post hoc testing (SYSTAT v.10.2, Point Richmond, CA). Results are expressed as mean ± the standard error of the mean (SEM) or standard deviation (SD), as indicated in the figure legends. Differences were considered statistically significant at $p<0.05$.

Results

Dynamic tensile loading rapidly induces chromatin condensation

Naive MSCs seeded onto aligned nanofibrous scaffolds were subjected to dynamic tensile loading (DL) with various frequencies and loading durations in the absence of exogenous soluble differentiation factors. 3% DL (applied at 0.2 Hz) resulted in chromatin condensation as visualized by alterations in DAPI staining intensity in nuclei (**Fig. 1A**). A similar increase in condensation was also observed with increased cell contractility when LPA (an activator of the small GTPase RhoA) was added to MSC cultures under loaded conditions (**Fig. 1A**). Conversely, when cellular contractility was reduced via treatment with Y27632 (Y27), an inhibitor of Rho-associated protein kinase (ROCK) or with ML7, an inhibitor of myosin light chain kinase, this load induced chromatin condensation was abolished (**Fig. 1A**). Note that the dose of ML7 used here was sufficient to decrease contractility while preserving the actin structure, while the dose of Y27 resulted in both a decrease in contractility and loss of stress fibers (22).

Quantification of chromatin condensation via the computation of a 'chromatin condensation parameter' (CCP) revealed increases of 70~80% compared to unloaded controls (No DL) in CM conditions when MSCs were exposed to 3% DL for 600 sec (**Fig. 1 B, sFig. 1B**). This increase in CCP was independent of the frequency of the applied DL. LPA treatment (for 15 min) increased the baseline CCP (**sFig. 1A**), with small increases from this higher level seen with increasing frequency and duration of loading (**Fig. 1B**). Conversely, when cell contractility was reduced via pre-treatment with Y27 or ML7,

chromatin condensation did not change with any loading condition. This suggests that acto-myosin contractility is required for load induced chromatin condensation (**Fig. 1B**).

Based on these findings, we re-plotted the data to determine whether there was a correlation between DL and CCP values as a function of the number of loading cycles applied. We found a strong positive correlation between the log of the number of cycles and the CCP value. This was true at every frequency of applied DL suggesting that there was no effect of loading rate in this situation (**sFig. 1C**). Cells that were pre-treated with LPA showed a higher baseline CCP and had a significantly lower slope relating the number of cycles and the CCP ($p=0.017$, LPA+DL in **sFig. 1C**). Pre-treatment with ML7 (ML7+DL in **sFig. 1C**) or Y27 (Y27+DL in **sFig. 1C**) resulted in a similar insensitivity to loading cycle number, albeit starting from a lower CCP value.

Extracellular ATP modulates load induced chromatin condensation

Having demonstrated that DL rapidly induced chromatin condensation in MSCs, we next investigated the time course of loading induced ATP release. To do so, DL (1 Hz) was applied to MSCs for different durations (5, 10, 20, or 30 sec) and ATP concentration in conditioned media was measured. In addition, to determine whether ATP release continued after this initial release, the media (1^{st} media) was switched to fresh media (2^{nd} media) after the cessation of each loading, and ATP concentration was measured in this fresh media after an additional free swelling period up to 600 sec. DL triggered rapid ATP release from MSCs, with the highest values observed after 10 sec. ATP concentration in the media (2^{nd} media) remained low for all loading conditions (**Fig. 2A**). In addition, we observed a ~50% decrease in the intensity of the quinacrine-stained ATP vesicles in MSCs after DL for 30 sec (1 Hz, **sFig. 2**). These data suggest that DL induces ATP release very rapidly, within 30 sec, and that little ATP is released after this point, even when DL is continued.

Given that DL triggers rapid ATP release from MSCs, we next investigated the role of extracellular ATP in the load-induced chromatin condensation. To do so, we evaluated the timing of ATP release and chromatin condensation in MSCs in response to DL. Compared to free-swelling conditions (a in **Fig. 2B-D**), application of 3% DL for 30 sec or 600 sec triggered ATP release from MSCs (determined in each conditioned media, c or d in **Fig. 2B, C**). However, as described above, increases in CCP values were only observed with DL applied for 600 sec (d in **Fig. 2B, D**) and not after only 30 sec (c in **Fig. 2B, D**). Increased ATP concentration in the media as a result of DL (30 sec) did not change with additional free swelling culture time up to 600 sec ($p>0.05$, e in **Fig. 2B, C**). Interestingly, with additional free swelling culture up to 600 sec, CCP values did increase after the cessation of DL (e in **Fig. 2B, D**). Furthermore, when we switched to fresh media immediately after the cessation of DL for 30 sec and measured ATP in the fresh media and CCP values at 600 sec, ATP in the fresh media remained low (f in **Fig. 2B, C**) but the CCP values still increased at 600 sec (f in **Fig. 2B, D**). In a control group, changing media alone to fresh CM media did not affect ATP concentration or CCP (**Fig. 2B-D**). The same was observed in groups where the media was switched to fresh media at 30 sec during continuous DL up to 600 sec (1 Hz, g in **Fig. 2B-D**). Similar results were observed when we applied DL at 0.2 Hz (**sFig. 3A-B**). These data suggest that DL induced release of ATP within the 30 sec of the start of loading, and that this early release was responsible for the marked increases in chromatin condensation that occur at a later point.

ATP synthase activity is required for the restoration of ATP filled vesicles

Having established that DL rapidly stimulates ATP release, we next sought to determine the rate at which ATP is replenished in MSCs after DL. This period would represent a 'refractory' period in these cells, during which additional ATP release would not be possible. To do so, we applied a second bout of DL (1 Hz, 30 sec) at time points of 1, 2, 3, 4, or 5 hours after the cessation of the 1st bout of DL (1 Hz, 30

sec). ATP release into the media was measured in each of these cases. The highest release occurred when the additional DL was applied 3 hours after the cessation of the 1st DL (**Fig. 3A**). However, for all groups, the levels of ATP release did not match the level measured in the media immediately after the 1st DL (**Fig 3A**). Somewhat consistent with these findings, the intensity of the quinacrine-stained ATP vesicles in MSCs decreased markedly after the 1st DL, but recovered to baseline levels within ~4 hours of free swelling (FS) culture after the cessation of the 1st DL (DL/FS 4h, **Fig. 3B**). Application of additional bout of DL after this 4 hour free swelling (DL/FS 4h/DL) culture decreased the intensity of this staining (**Fig. 3B**). Restoration of these intracellular ATP stores could be blocked by inhibition of F_1F_o. Inhibition of mitochondrial H+ transport coupled to ATP synthesis with either oligomycin (Olig) or dicyclohexylcarbodiimide (DCC), added to the media after 1st DL, resulted in a failure to induce an ATP release with additional loading. This indicates that ATP synthase in mitochondria is required for recovery of ATP stores within the cell after the application of the first DL (**Fig. 3C**).

Cellular contractility is essential for load induced ATP release

Given that many studies (20) have established that mechanical perturbation activates RhoA/ROCK signaling (which regulates cellular contractility), leading to ATP release from many types of cells and changes in Ca^{2+} signaling, we next determined how dampening of this pathway via treatment with pharmacological inhibitors might influence load induced ATP release and $[Ca^{2+}]_i$ signaling. Consistent with our previous findings (16), DL (3%, 30 sec) triggered ATP release from MSCs (**sFig. 4**) across a range of frequencies (0.2 ~ 0.2 Hz). Similarly, when contractility was increased via treatment with LPA, ATP release was activated within 5 sec, with levels plateauing after 30 sec (**Fig. 4A**). In addition, LPA treatment increased the fraction of MSCs showing $[Ca^{2+}]_i$ oscillations (**Fig. 4B**) and the number of $[Ca^{2+}]_i$ peaks during a 10 min observation period (**Fig. 4C**). Conversely, when MSCs were pre-treated with ML7 or Y27 to reduce baseline cellular contractility, ATP release did not occur during DL (**Fig. 4D**).

Furthermore, decreasing contractility by inhibition of either myosin light chain kinase (with ML7) or ROCK (with Y27) prevented any changes in $[Ca^{2+}]_i$ oscillations in response to mechanical perturbation (3% grip-to-grip static stretch) (E: % responding cells, F: number of peaks, **Fig. 4E-F**). Basal cellular contractility was also required for increases in chromatin condensation with the addition of exogenous ATP. Addition of a high concentration of ATP increased chromatin condensation (CCP, **Fig. 4G**), the fraction of the population showing $[Ca^{2+}]_i$ oscillations (**Fig. 4H**), and the number of peaks during the observation period (**Fig. 4I**). However, when contractility was decreased by pre-treatment with MLCK or Rho inhibitors, no condensation and no changes in $[Ca^{2+}]_i$ oscillations was observed with ATP addition (**Fig. 4G-I**).

Taken together, these data suggest that mechanical loading triggers ATP release and that this is a mediator of chromatin condensation in MSCs. Likewise, the action of ATP appears to depend on contractility, given that the response of exogenous addition of a high concentration of ATP was blocked in Y27 and ML7 treated cells.

TGF-β superfamily signaling is essential for load induced chromatin condensation

It is well known that TGF-β superfamily members, including TGF-β and BMP, are involved in many cellular functions, including cell migration, proliferation, and differentiation (24-26, 38). Exogenous mechanical cues can also regulate signaling in this pathway (39). To explore the potential role of TGF-β superfamily signaling in load induced chromatin condensation, inhibitors of this pathway were applied for 2 hours prior to and during DL (1Hz, 3%, 600 sec). Pharmacological inhibitors for the TGF-β superfamily included SB431542 (SB) to inhibit the TGF-β pathway or LDN193189 (LDN) to inhibit BMP pathway (**Fig. 5A**). After the cessation of DL, CCP was determined. Also, DL conditioned media were collected to measure ATP or were added to naive (unloaded) MSC-seeded constructs followed by determination of CCP (**Fig. 5A**). When DL was applied with blockade of either TGF-β or BMP signaling

(SB/DL or LDN/DL), DL induced chromatin condensation was abolished (**Fig. 5B**). Further, the addition of DL conditioned media increased CCP values in unloaded MSC-seeded constructs (**Fig. 5C**), while the addition of media collected from SB or LDN pre-treated groups did not change chromatin condensation in these unloaded MSCs (**Fig. 5C**). Consistent with our previous findings (16), DL (3%, 1Hz, 600s) triggered ATP release into the media (**Fig. 5D**). However, pretreatment with SB or LDN blocked this ATP release (**Fig. 5D**). To probe additional downstream responses, we also monitored $[Ca^{2+}]_i$ oscillations in MSCs (**Fig. 5E-F**): changes in the percent responding cells and the number of peaks in response to 3% static stretch were all attenuated by inhibition of TGF or BMP signaling (**Fig. 5E-F**). Collectively, these finding suggest that blockade of TGF-β superfamily signaling attenuates the release of ATP and blocks the activation of calcium signaling upon DL, short-circuiting the load induced chromatin condensation events that would otherwise occur.

Blockade of TGF-β/BMP signaling reduces baseline cellular contractility

Given that inhibition of TGF-β/BMP signaling blocked DL-induced ATP release and chromatin condensation, we next sought to determine whether inhibition of these pathways via pre-treatment with SB or LDN decreased cellular contractility to the point where insufficient stress was generated in the cytoskeleton, and whether this was the cause for the loss in mechanically induced ATP release with DL. To answer this question, traction force generated by MSCs was measured after pharmacological inhibition of the TGF/BMP SMAD pathways. Traction force maps for single cells showed a marked decrease in traction with the addition of SB, LDN or Y27 compared to controls in CM conditions (**Fig. 6A**). Quantitatively, inhibition SMAD 2/3 or SMAD 1/5/8 (with addition of SB or LDN, respectively) decreased total force generated per cell by 60-90% (**Fig. 6B, sFig. 6A**) and the average traction stress per cell by 60-70% compared to controls in CM conditions, reaching levels similar to addition of Y27 (**Fig. 6C, sFig. 6B**). Cell area did not change with pharmacological inhibition (**s.Fig. 7**). Interestingly,

activation of these pathways seemed to occur in the absence of ligand, since cell traction was unaffected when we applied neutralizing antibodies to TGF-β (**sFig. 8A, B**). These findings indicate that, even in the absence of ligands, inhibition of TGF-β/BMP signaling decreases baseline cellular contractility in MSCs, lessening their response to DL.

DISCUSSION

In this study, we demonstrated that dynamic tensile loading leads to rapid chromatin condensation in MSCs on aligned nanofibrous scaffolds in the absence of exogenous differentiation factors. In addition, we showed that extracellular ATP release in response to mechanical stimulation is a key early regulator of this chromatin condensation. Indeed, it appears that a burst release of ATP (within 30 sec of loading onset) is sufficient to mediate subsequent changes in chromatin condensation that culminate by 600 seconds. This suggests that stretch couples with events initiated by ATP release to promote condensation. Indeed, the mechanically induced chromatin condensation required acto-myosin contractility, in agreement with other studies (39). It is likely that ATP release stimulates P2 receptors and calcium ion channels, resulting in increased Ca^{2+} influx into cells (40). Binding of Ca^{2+} to calcium binding proteins, such as calmodulin and calcineurin, activate transcription and modify chromatin (41, 42). Likewise, exogenous ATP activates G protein-coupled P2Y receptors, leading to the activation of RhoA GTPases, which in turn increase cellular contractility (43) and vice versa (44). Other cell types have also been shown to regulate RhoA GTPase activation through activation of ATP-related purinergic signaling, or via the application of various forms of mechanical stimuli (23).

Our data indicate that dynamic loading increases ATP release, which might be mediated by RhoA GTPase activation in MSCs. Previously we reported that load induced chromatin condensation was abrogated with removal of extracellular ATP or by inhibition of ATP release (16). Here, we show that chromatin condensation in MSCs occurs as a consequence of just 30 sec of DL, and that this is abolished

with treatment with a ROCK inhibitor, Y27 or an inhibitor of myosin activation, ML7. Furthermore, LPA or Y27 or ML7 treated cells were no longer susceptible to loading-induced chromatin condensation. This may be because treatment with LPA led to a burst release and depletion of ATP-stores, and insufficient myosin-II activity with treatment of Y27 or ML7 affected cell mechanosensitivity. Together these data suggest that rapidly released ATP, in response to DL, requires cell contractility for mechanically regulated chromatin remodeling. Furthermore, we show that these internal ATP stores are gradually restored after the initial burst release with short term DL, and that this restoration is abolished by treatment with inhibitors of ATP synthase (oligomycin or dicyclohexylcarbodiimide) located on the inner mitochondrial membrane. This suggests that ATP synthesis in mitochondria is required for cells to maintain their mechano-sensitivity in the context of repeated loading events. Interestingly, when a high level of exogenous ATP was added to cells pre-treated with contractility antagonists, chromatin condensation was also blocked. This finding supports the idea that mechanically induced ATP signaling depends on cellular contractility for both initiation and propagation of the transduction event.

Transforming growth factor beta (TGF-β) superfamily members, including TGF-β and BMP, are a large family of regulatory proteins controlling proliferation, differentiation and other functions in many cell types (24-26, 38). These proteins interact with specific protein kinase receptors, including type I and the type II serine/threonine receptor kinases, which become activated upon ligand binding (45). This event generates intracellular signaling through the phosphorylation of SMAD proteins (45). Recent studies have shown that various types of mechanical stimuli also modulate TGF-β/BMP signaling and SMAD phosphorylation (39). For example, Zang et al reported that dynamic compression activated pSMAD2/3 and induced chondrogenesis of MSCs (46) and Kearney et al showed that cyclic uniaxial tensile strain enhanced BMP2 and osteocalcin expression through activation of pSMADs (47). Furthermore, the TGF-β superfamily is closely correlated with RhoA/Rho-associated protein kinase (ROCK) activity and regulation of cellular contractility. For example, Wang et el. showed that BMP release induced by changing cell shape and substrate mechanics can result in SMAD phosphorylation.

This resulted in rapid and sustained RhoA/Rho-associated protein kinase (ROCK) activation, increasing cellular tension (48) and inducing osteogensis of human mesenchymal stem cells (48). This differentiation could be blocked when cellular tension was abrogated. This suggests that TGF/BMP ligand binding induces phosphorylation of SMADs and regulates cellular contractility, mediated through ROCK and myosin signaling, and that this in turn can modulate MSC differentiation. Taken together, it is clear that the mechanically regulated SMAD signaling can activate RhoA/ROCK signaling, although the role that SMAD signaling on its own plays in establishing cellular contractility and how this impacts mechanically activated purinergic signaling remains to be determined.

Towards this open question, we show here that the TGF-β superfamily is a key pathway in regulating loading induced chromatin condensation. Inhibition of pSMAD 2/3 (TGF) signaling using SB431542 or pSMAD 1/5/8 (BMP) signaling using LDN193189 abrogated load induced chromatin condensation. This is not surprising given that mechanical forces may trigger the release and activation of latent TGF-β in the surrounding ECM, which may induce chromatin condensation via autocrine signaling. Blockade of TGF-β superfamily signaling also resulted in the interruption of mechanically induced ATP release and $[Ca^{2+}]_i$ influx, which blocked load-induced chromatin condensation. It is also possible that inhibition of these intracellular SMADs affected basic cellular metabolism. Indeed, application of the pharmacologic inhibitors to inhibit SMAD 2/3 or SMAD 1/5/8 resulted in significant decreases in cellular contractility. Interestingly, neutralizing antibodies to TGF-β did not alter baseline contractility suggesting that activation occurs in a 'leaky' fashion. These data suggests that SMAD signaling may play important roles in regulating baseline cellular contractility, even in the absence of exogenous ligands, and that this may be the mechanism by which this pathway regulates load-induced ATP release and chromatin condensation.

In summary, our findings further explicate the molecular mechanisms of mechanically induced chromatin condensation in MSCs. We directly implicate ATP/purinergic signaling in MSC response to DL through the RhoA-ROCK pathway. Our data also indicate that chromatin condensation is regulated by

TGFβ/BMP signaling, through the establishment of a baseline level of cellular contractility, which in turn tunes their mechanosensitivity and responsiveness to mechanical perturbation (**Fig.7**).

AUTHOR CONTRIBUTIONS

SJH, WMH, SES, BDC, DME, DAL, RLD, and RLM designed the studies. SJH, WMH, SES and BDC performed the experiments. SJH, WMH, SES, BDC, DME, DAL, RLD, and RLM analyzed and interpreted the data. SJH, WMH, SES, and RLM drafted the manuscript, and all authors edited the final submission.

ACKNOWLEDGMENTS

This work was supported by the National Institutes of Health (R01 AR056624, R01 EB02425, T32 AR007132, and P30 AR050950). Additional support was provided by a Montague Research Award from the Perelman School of Medicine and a University of Pennsylvania University Research Foundation Award. The authors would like to acknowledge technical contributions to this work from Dr. Stephen D. Thorpe, and J. Caplan for assistance with confocal microscopy.

Figure legends

Figure 1. Chromatin remodeling occurs rapidly in response to dynamic tensile loading (DL), and depends on the contractile cytoskeleton. (A) In the absence of exogenous growth factors and with/without pre-treatment of LPA (an activator of G-protein coupled receptors), DL (3%, 0.2 Hz) for 600s increases chromatin condensation and increases the number of visible edges in nuclei. When MSCs were pre-treated with a MLCK inhibitor (ML7) or a Rho-kinase inhibitor (Y27) prior to the application of DL, no significant changes in chromatin condensation were observed with DL (left: DAPI stained nuclei, right: corresponding edge detection, bar = 3 μm). (**B**) Heat map showing quantification of the chromatin condensation parameter (CCP) in response to DL (CM+DL), with addition of LPA (LPA+DL) or with

inhibition of acto-myosin contractility via ML7 (ML7+DL) or Y27 (Y27+DL) pre-treatment (n = ~ 55 cells per condition per time point, from 3 replicate studies, each value indicates mean with the standard deviations shown in supplemental figure 1B, *: $p<0.05$ vs. CM without DL, +: $p<0.05$ vs. 0.2 Hz, ‡: $p<0.05$ vs. 0.5 Hz).

Figure 2. Dynamic loading triggers ATP release, which mediates chromatin condensation in MSCs. (A) Assessment of ATP concentration in the 1st media collected after cessation of short term DL (1Hz, 3%) with various durations (5 sec, 10 sec, 20 sec, or 30 sec) or in the 2nd replacement media (that was switched and cultured for an additional 600s after cessation of each DL) (normalized to ATP concentration in CM condition: 76 nM , *: $p<0.05$ vs. CM conditions in red line, +: $p<0.05$ vs. 1st media with DL for 5 sec, #: $p<0.05$ vs. 1st media with DL for 10 sec, α: $p<0.05$ vs., 1st media with DL for 20 sec, β: $p<0.05$ vs. 1st media with DL for 30 sec, mean ± SD). (B) Schematic showing experimental setup. (C) ATP concentration in conditioned media (normalized to ATP concentration in CM condition: 65 nM, red line, mean ± SD) and (D) CCP values under various conditions [a: CM media for 600s without DL, b: CM media for 30 sec followed by switching to new fresh media up to 600 sec without DL, c: DL condition (1 Hz, 3%, 30 sec), d: DL condition (1 Hz, 3%, 600 sec), e: DL condition (1 Hz, 3%, 30 sec) followed by free swelling up to 600 sec, f: DL condition (1 Hz, 3%, 30 sec) followed by free swelling up to 600 sec in fresh media, g: DL condition (1 Hz, 3%, 600 sec) with fresh media applied at 30 sec, n = 3 from 3 biological replicates for (C), n = ~35 for (D), *: $p<0.05$ vs. a, mean ± SEM].

Figure 3. ATP content and release capacity is gradually restored after DL via ATP synthase activity in mitochondria. (A) Measurement of ATP release when an additional DL event is applied after the 1st DL event (normalized to the ATP concentration in CM conditions: 88 nM, DL: 1 Hz, 3%, 30 sec, blue line: ATP release by the 1st DL, red line: ATP concentration in CM conditions, n = 3 from 3 biological replications, +: $p<0.05$ vs. CM conditions, *: $p<0.05$ vs. 1h, mean ± SD). (B) Quantification of quinacrine dihydrochloride staining of ATP-filled vesicles in MSCs after 1st DL (DL), 1 hour after 1st DL (DL/FS 1h), 4 hours after 1st DL (DL/FS 4h), 4 hours after 1st DL followed by an additional DL (DL/FS 4h/DL) (normalized to intensity in CM conditions, DL: 1 Hz, 3%, 30 sec, FS: free swelling, n = 3 from 3 biological replications, *: $p<0.05$ vs. CM conditions in red line, mean ± SEM). (C) ATP release by an additional DL that was applied 4h after the 1st DL with/without treatment with ATP synthase inhibitors (normalized to ATP concentration in CM media: 76 nM, Oligo: oligomycin, DCC: dicyclohexylcarbodiimide, n = 3 from 3 biological replicates, *: $p<0.05$ vs. CM conditions in red line, +: $p<0.05$ vs. 1st DL 30 sec in blue line, α: $p<0.05$ vs. CM conditions, mean ± SD).

Figure 4. Mechanically induced ATP release is mediated by cellular contractility. (A) ATP release after LPA treatment or with application of DL (normalized to ATP concentration in CM conditions 55 nM, DL: 1 Hz, 3%, 30 sec, blue line: DL conditions, red line: CM conditions, n = 3 from 3 biological replicates, *: $p<0.05$ vs. CM conditions, mean ± SD). (B-C) $[Ca^{2+}]_i$ oscillations with LPA treatment (B: % responding cells, C: number of peaks in 10 min observation window, green line: response to 3% static stretch in CM conditions, *: $p<0.05$ vs. CM conditions, mean ± SD). (D) ATP release with the application of DL (CM+DL) with/without ML7 (ML7+DL) or Y27 (Y27+DL) pre-treatment (normalized to ATP

concentration in no DL media, DL: 1 Hz, 3%, 30 sec, red line: CM conditions, n = 3 from 3 biological replicates, *: $p<0.05$ vs. CM conditions, mean ± SD). (E-F) $[Ca^{2+}]_i$ oscillations with 3% static stretch (relative to values in 0% stretch conditions, E: % responding cells, F: number of peaks in 10 min observation window, red line: CM conditions, n = ~ 30 cells, *: $p<0.05$ vs. CM conditions in red, mean ± SD). (G) CCP values with the addition of exogenous ATP (300 μM for 30 mins) with/without pre-treatment with ML7 or Y27 (normalized to CCP in CM media, n = ~ 20, *: $p<0.05$ vs. CM conditions in red line, mean ± SEM). (H-I) $[Ca^{2+}]_i$ oscillations in MSCs with the addition of exogenous ATP (300 μM) with/without pre-treatment with ML7 or Y27 (relative to values in CM conditions H: % responding cells, I: number of peaks in 10 min observation window, red line: CM conditions, n = ~ 30 cells, *: $p<0.05$ vs. CM conditions in red, mean ± SD).

Figure 5. TGFβ/BMP signaling regulates load-induced chromatin condensation. (A) Schematic illustration of conditioned media studies including pre-treatment with inhibitors of TGFβ/BMP signaling pathways (SB: SB431542, LDN: LDN193189). (B) Normalized CCP values in load-induced MSCs (relative to unloaded MSCs in CM conditions) after the cessation of DL (1 Hz, 3%, 600 sec) with/without pre-treatment with SB or LDN (n = ~20, *: $p<0.05$ vs. CM conditions in red line, mean ± SEM). (C) Normalized CCP in free swelling MSCs (relative to values in CM conditions) after treatment for 30 minutes with DL-conditioned media (n = ~20, *: $p<0.05$ vs. CM conditions in red line, mean ± SEM). (D) Increases in ATP concentration in media after DL for 600 sec does not occur in SB/LDN pre-treated conditions (normalized to CM conditions in red line: 71 nM, n = 3 from 3 biological replications, *: $p<0.05$ vs. CM conditions, mean ± SD). (E-F) $[Ca^{2+}]_i$ oscillations in MSCs in response to 3% static stretch with/without pre-treatment with SB or LDN (E: % responding cells, F: number of peaks in 10 min observation window, n = ~ 30 cells, *: $p<0.05$ vs. CM conditions in red, mean ± SD).

Figure 6. Baseline traction force in MSCs is established by ligand-less TGFβ/BMP signaling. (A) Traction force maps for MSCs on 10 kPa polyacrylamide gels with/without addition of SB or LDN or Y27 (Quantification of total force per cell, line: cell border, bar = 25 μm), (B) and the ratio of strain energy per cell spread area (n=16~31 cells per group, * $p<0.05$ vs. CM conditions, mean ± SEM).

Figure 7. Schematic outlining the signaling pathways controlling mechanically induced chromatin condensation. Actomyosin-based cellular contractility is critical for mechanically induced chromatin condensation in MSCs. Dynamic loading (DL) induces ATP release within 30 sec and depends on baseline cellular contractility. This ATP release in turn activates P2Rs (P2 receptors) and the resultant increase in intracellular Ca^{2+} activates the Rho/ROCK signaling pathway and cell contractility, amplifying the load-induced mechanical response. This ultimately culminates at longer time points in alterations in chromatin condensation. While the precise mechanism remains undefined, inhibition of the transforming growth factor-β (TGF-β) superfamily decreases baseline cellular contractility, blocking the first step in load-induced chromatin condensation response. Solid lines: defined pathways, dashed-lines: undefined pathways.

References

1. Bianco, P., X. Cao, P.S. Frenette, J.J. Mao, P.G. Robey, P.J. Simmons, and C.Y. Wang 2013. The meaning, the sense and the significance: translating the science of mesenchymal stem cells into medicine. *Nat Med.* 19: 35-42.
2. Pittenger, M.F., A.M. Mackay, S.C. Beck, R.K. Jaiswal, R. Douglas, J.D. Mosca, M.A. Moorman, D.W. Simonetti, S. Craig, and D.R. Marshak 1999. Multilineage potential of adult human mesenchymal stem cells. *Science.* 284: 143-147.
3. Nava, M.M., M.T. Raimondi, and R. Pietrabissa 2012. Controlling self-renewal and differentiation of stem cells via mechanical cues. *J Biomed Biotechnol.* 2012: 797410.
4. Taniguchi, N., B. Carames, E. Hsu, S. Cherqui, Y. Kawakami, and M. Lotz 2011. Expression patterns and function of chromatin protein HMGB2 during mesenchymal stem cell differentiation. *J Biol Chem.* 286: 41489-41498.
5. Bannister, A.J., and T. Kouzarides 2011. Regulation of chromatin by histone modifications. *Cell Res.* 21: 381-395.
6. Binder, H., L. Steiner, J. Przybilla, T. Rohlf, S. Prohaska, and J. Galle 2013. Transcriptional regulation by histone modifications: towards a theory of chromatin re-organization during stem cell differentiation. *Phys Biol.* 10: 026006.
7. Fukuda, H., N. Sano, S. Muto, and M. Horikoshi 2006. Simple histone acetylation plays a complex role in the regulation of gene expression. *Brief Funct Genomic Proteomic.* 5: 190-208.
8. Fullgrabe, J., N. Hajji, and B. Joseph 2010. Cracking the death code: apoptosis-related histone modifications. *Cell Death Differ.* 17: 1238-1243.
9. Zullo, J.M., I.A. Demarco, R. Pique-Regi, D.J. Gaffney, C.B. Epstein, C.J. Spooner, T.R. Luperchio, B.E. Bernstein, J.K. Pritchard, K.L. Reddy, and H. Singh 2012. DNA sequence-dependent compartmentalization and silencing of chromatin at the nuclear lamina. *Cell.* 149: 1474-1487.
10. Gaspar-Maia, A., A. Alajem, E. Meshorer, and M. Ramalho-Santos 2011. Open chromatin in pluripotency and reprogramming. *Nat Rev Mol Cell Biol.* 12: 36-47.
11. Schneider, R., and R. Grosschedl 2007. Dynamics and interplay of nuclear architecture, genome organization, and gene expression. *Genes Dev.* 21: 3027-3043.
12. Baker, B.M., R.P. Shah, A.H. Huang, and R.L. Mauck 2011. Dynamic tensile loading improves the functional properties of mesenchymal stem cell-laden nanofiber-based fibrocartilage. *Tissue Eng Part A.* 17: 1445-1455.
13. Li, Y., J.S. Chu, K. Kurpinski, X. Li, D.M. Bautista, L. Yang, K.L. Sung, and S. Li 2011. Biophysical regulation of histone acetylation in mesenchymal stem cells. *Biophys J.* 100: 1902-1909.
14. Irianto, J., J. Swift, R.P. Martins, G.D. McPhail, M.M. Knight, D.E. Discher, and D.A. Lee 2013. Osmotic challenge drives rapid and reversible chromatin condensation in chondrocytes. *Biophys J.* 104: 759-769.
15. Irianto, J., D.A. Lee, and M.M. Knight 2014. Quantification of chromatin condensation level by image processing. *Medical engineering & physics.* 36: 412-417.
16. Heo, S.J., S.D. Thorpe, T.P. Driscoll, R.L. Duncan, D.A. Lee, and R.L. Mauck 2015. Biophysical Regulation of Chromatin Architecture Instills a Mechanical Memory in Mesenchymal Stem Cells. *Sci Rep.* 5: 16895.

17. Mih, J.D., A. Marinkovic, F. Liu, A.S. Sharif, and D.J. Tschumperlin 2012. Matrix stiffness reverses the effect of actomyosin tension on cell proliferation. *J Cell Sci.* 125: 5974-5983.
18. Yim, E.K., and M.P. Sheetz 2012. Force-dependent cell signaling in stem cell differentiation. *Stem Cell Res Ther.* 3: 41.
19. Hirata, H., M. Gupta, S.R. Vedula, C.T. Lim, B. Ladoux, and M. Sokabe 2015. Actomyosin bundles serve as a tension sensor and a platform for ERK activation. *EMBO Rep.* 16: 250-257.
20. Provenzano, P.P., and P.J. Keely 2011. Mechanical signaling through the cytoskeleton regulates cell proliferation by coordinated focal adhesion and Rho GTPase signaling. *J Cell Sci.* 124: 1195-1205.
21. Iyer, K.V., S. Pulford, A. Mogilner, and G.V. Shivashankar 2012. Mechanical activation of cells induces chromatin remodeling preceding MKL nuclear transport. *Biophys J.* 103: 1416-1428.
22. Driscoll, T.P., B.D. Cosgrove, S.J. Heo, Z.E. Shurden, and R.L. Mauck 2015. Cytoskeletal to Nuclear Strain Transfer Regulates YAP Signaling in Mesenchymal Stem Cells. *Biophys J.* 108: 2783-2793.
23. Gardinier, J., W. Yang, G.R. Madden, A. Kronbergs, V. Gangadharan, E. Adams, K. Czymmek, and R.L. Duncan 2014. P2Y2 receptors regulate osteoblast mechanosensitivity during fluid flow. *Am J Physiol Cell Physiol.* 306: C1058-1067.
24. Burks, T.N., and R.D. Cohn 2011. Role of TGF-beta signaling in inherited and acquired myopathies. *Skelet Muscle.* 1: 19.
25. Chen, G., C. Deng, and Y.P. Li 2012. TGF-beta and BMP signaling in osteoblast differentiation and bone formation. *Int J Biol Sci.* 8: 272-288.
26. Itman, C., C. Wong, P.A. Whiley, D. Fernando, and K.L. Loveland 2011. TGFbeta superfamily signaling regulators are differentially expressed in the developing and adult mouse testis. *Spermatogenesis.* 1: 63-72.
27. Heo, S.J., N.L. Nerurkar, B.M. Baker, J.W. Shin, D.M. Elliott, and R.L. Mauck 2011. Fiber stretch and reorientation modulates mesenchymal stem cell morphology and fibrous gene expression on oriented nanofibrous microenvironments. *Ann Biomed Eng.* 39: 2780-2790.
28. Nathan, A.S., B.M. Baker, N.L. Nerurkar, and R.L. Mauck 2011. Mechano-topographic modulation of stem cell nuclear shape on nanofibrous scaffolds. *Acta Biomater.* 7: 57-66.
29. Mauck, R.L., X. Yuan, and R.S. Tuan 2006. Chondrogenic differentiation and functional maturation of bovine mesenchymal stem cells in long-term agarose culture. *Osteoarthritis Cartilage.* 14: 179-189.
30. Han, W.M., S.J. Heo, T.P. Driscoll, M.E. Boggs, R.L. Duncan, R.L. Mauck, and D.M. Elliott 2014. Impact of cellular microenvironment and mechanical perturbation on calcium signalling in meniscus fibrochondrocytes. *Eur Cell Mater.* 27: 321-331.
31. Godbout, C., L. Follonier Castella, E.A. Smith, N. Talele, M.L. Chow, A. Garonna, and B. Hinz 2013. The mechanical environment modulates intracellular calcium oscillation activities of myofibroblasts. *PLoS One.* 8: e64560.
32. Kim, T.J., J. Sun, S. Lu, Y.X. Qi, and Y. Wang 2014. Prolonged mechanical stretch initiates intracellular calcium oscillations in human mesenchymal stem cells. *PLoS One.* 9: e109378.
33. Genetos, D.C., D.J. Geist, D. Liu, H.J. Donahue, and R.L. Duncan 2005. Fluid shear-induced ATP secretion mediates prostaglandin release in MC3T3-E1 osteoblasts. *J Bone Miner Res.* 20: 41-49.
34. Fillingame, R.H. 1997. Coupling H+ transport and ATP synthesis in F1F0-ATP synthases: glimpses of interacting parts in a dynamic molecular machine. *J Exp Biol.* 200: 217-224.
35. Antoniel, M., V. Giorgio, F. Fogolari, G.D. Glick, P. Bernardi, and G. Lippe 2014. The oligomycin-sensitivity conferring protein of mitochondrial ATP synthase: emerging new roles in mitochondrial pathophysiology. *Int J Mol Sci.* 15: 7513-7536.
36. Scarborough, G.A. 1986. A chemically explicit model for the molecular mechanism of the F1F0 H+-ATPase/ATP synthases. *Proc Natl Acad Sci U S A.* 83: 3688-3692.

37. Tseng, Q., E. Duchemin-Pelletier, A. Deshiere, M. Balland, H. Guillou, O. Filhol, and M. Thery 2012. Spatial organization of the extracellular matrix regulates cell-cell junction positioning. *Proc Natl Acad Sci U S A.* 109: 1506-1511.
38. Leask, A., and D.J. Abraham 2004. TGF-beta signaling and the fibrotic response. *FASEB J.* 18: 816-827.
39. Saha, S., L. Ji, J.J. de Pablo, and S.P. Palecek 2008. TGFbeta/Activin/Nodal pathway in inhibition of human embryonic stem cell differentiation by mechanical strain. *Biophys J.* 94: 4123-4133.
40. Omatsu-Kanbe, M., T. Isono, and H. Matsuura 2002. Multiple P2 receptors contribute to a transient increase in intracellular Ca2+ concentration in ATP-stimulated rat brown adipocytes. *Exp Physiol.* 87: 643-652.
41. Bouvard, D., and M.R. Block 1998. Calcium/calmodulin-dependent protein kinase II controls integrin alpha5beta1-mediated cell adhesion through the integrin cytoplasmic domain associated protein-1alpha. *Biochem Biophys Res Commun.* 252: 46-50.
42. Hama, N., F. Paliogianni, B.J. Fessler, and D.T. Boumpas 1995. Calcium/calmodulin-dependent protein kinase II downregulates both calcineurin and protein kinase C-mediated pathways for cytokine gene transcription in human T cells. *J Exp Med.* 181: 1217-1222.
43. Erb, L., and G.A. Weisman 2012. Coupling of P2Y receptors to G proteins and other signaling pathways. *Wiley Interdiscip Rev Membr Transp Signal.* 1: 789-803.
44. Blum, A.E., S.M. Joseph, R.J. Przybylski, and G.R. Dubyak 2008. Rho-family GTPases modulate Ca(2+) -dependent ATP release from astrocytes. *Am J Physiol Cell Physiol.* 295: C231-241.
45. Wrighton, K.H., X. Lin, and X.H. Feng 2009. Phospho-control of TGF-beta superfamily signaling. *Cell Res.* 19: 8-20.
46. Zhang, T., F. Wen, Y. Wu, G.S. Goh, Z. Ge, L.P. Tan, J.H. Hui, and Z. Yang 2015. Cross-talk between TGF-beta/SMAD and integrin signaling pathways in regulating hypertrophy of mesenchymal stem cell chondrogenesis under deferral dynamic compression. *Biomaterials.* 38: 72-85.
47. Kearney, E.M., E. Farrell, P.J. Prendergast, and V.A. Campbell 2010. Tensile strain as a regulator of mesenchymal stem cell osteogenesis. *Ann Biomed Eng.* 38: 1767-1779.
48. Wang, Y.K., X. Yu, D.M. Cohen, M.A. Wozniak, M.T. Yang, L. Gao, J. Eyckmans, and C.S. Chen 2012. Bone morphogenetic protein-2-induced signaling and osteogenesis is regulated by cell shape, RhoA/ROCK, and cytoskeletal tension. *Stem Cells Dev.* 21: 1176-1186.

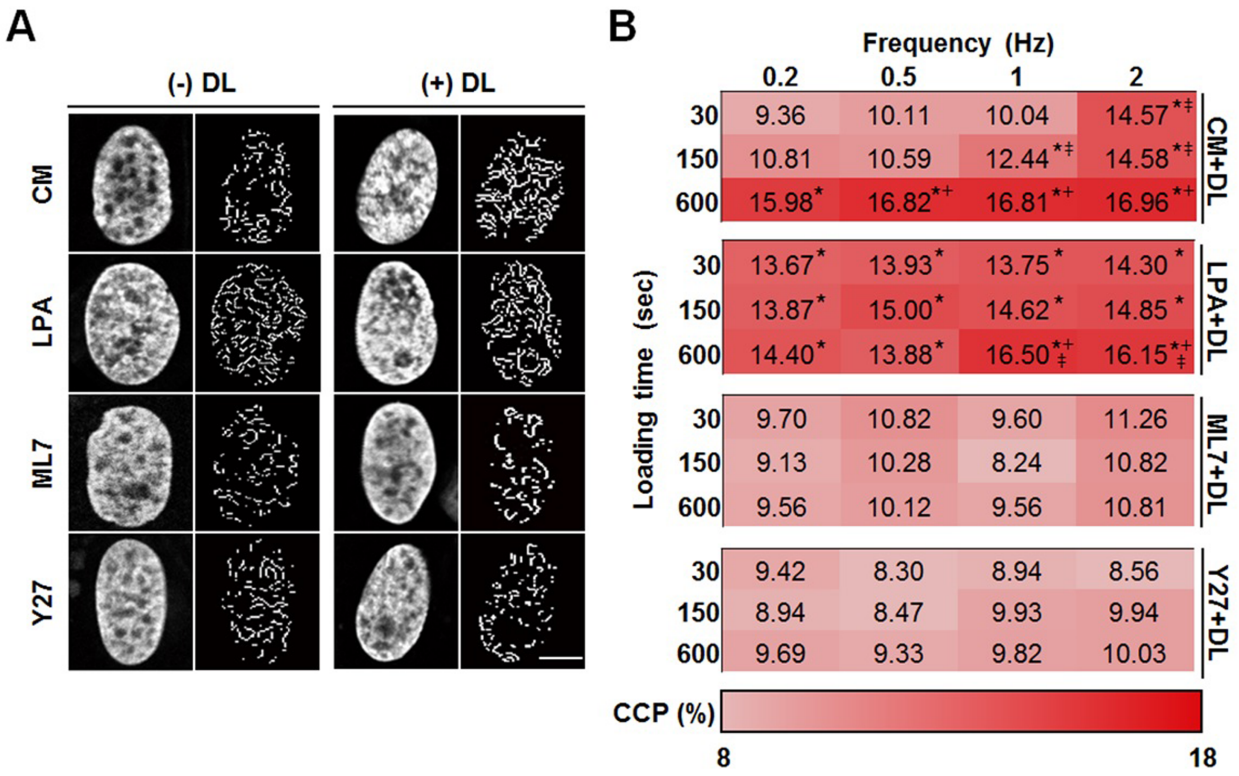
A
(-) DL
(+) DL
CM
LPA
ML7
Y27
B
Frequency (Hz)
0.2
0.5
1
2
Loading time (sec)
30
150
600
9.36
10.11
10.04
14.57*‡
10.81
10.59
12.44*‡
14.58*‡
15.98*
16.82*+
16.81*+
16.96*+
CM+DL
13.67*
13.93*
13.75*
14.30*
13.87*
15.00*
14.62*
14.85*
14.40*
13.88*
16.50*+‡
16.15*+‡
LPA+DL
9.70
10.82
9.60
11.26
9.13
10.28
8.24
10.82
9.56
10.12
9.56
10.81
ML7+DL
9.42
8.30
8.94
8.56
8.94
8.47
9.93
9.94
9.69
9.33
9.82
10.03
Y27+DL
CCP (%)
8
18

Figure 1

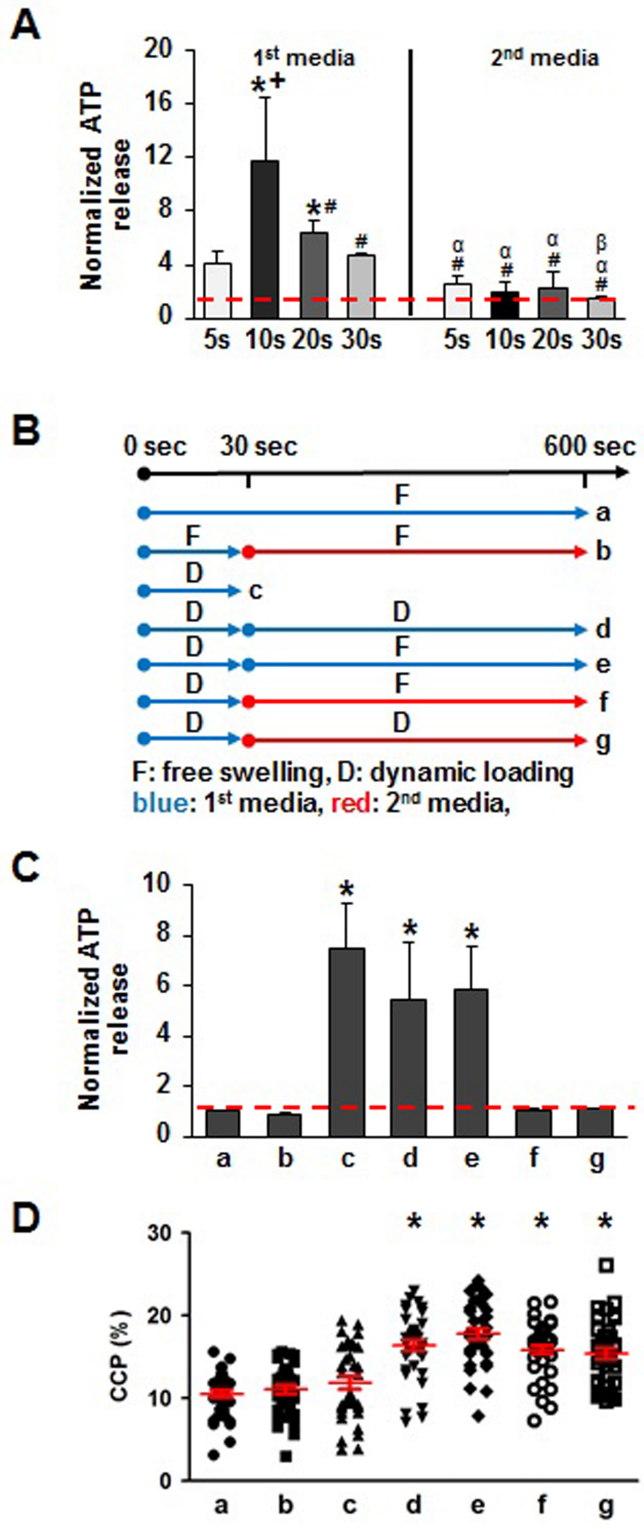
A
Normalized ATP release
1st media
2nd media
5s 10s 20s 30s
5s 10s 20s 30s
B
0 sec
30 sec
600 sec
F: free swelling, D: dynamic loading
blue: 1st media, red: 2nd media,
C
Normalized ATP release
a b c d e f g
D
CCP (%)
a b c d e f g

Figure 2

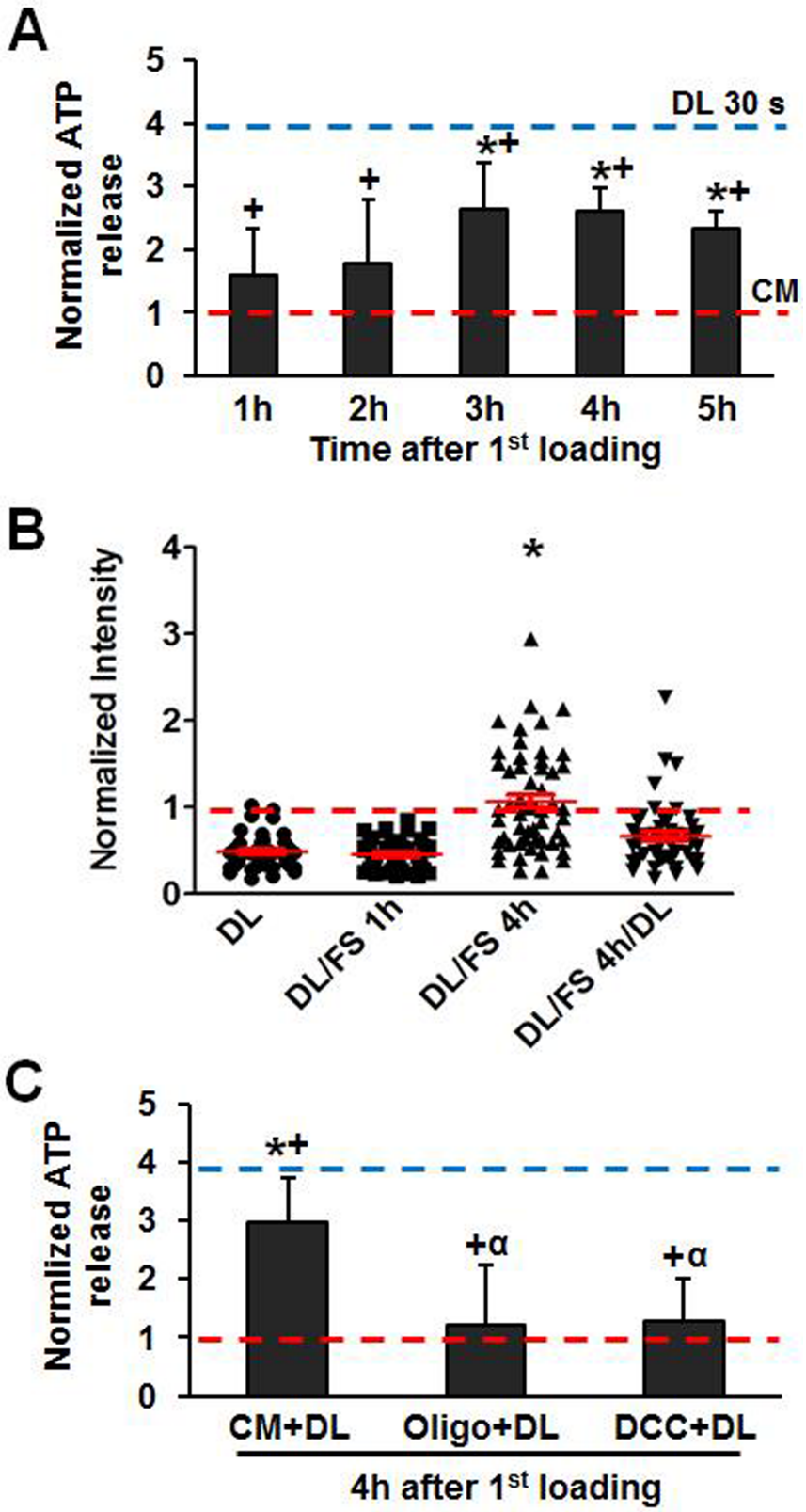
A
Normalized ATP release
DL 30 s
CM
1h
2h
3h
4h
5h
Time after 1st loading
B
Normalized Intensity
DL
DL/FS 1h
DL/FS 4h
DL/FS 4h/DL
C
Normlized ATP release
CM+DL
Oligo+DL
DCC+DL
4h after 1st loading

Figure 3

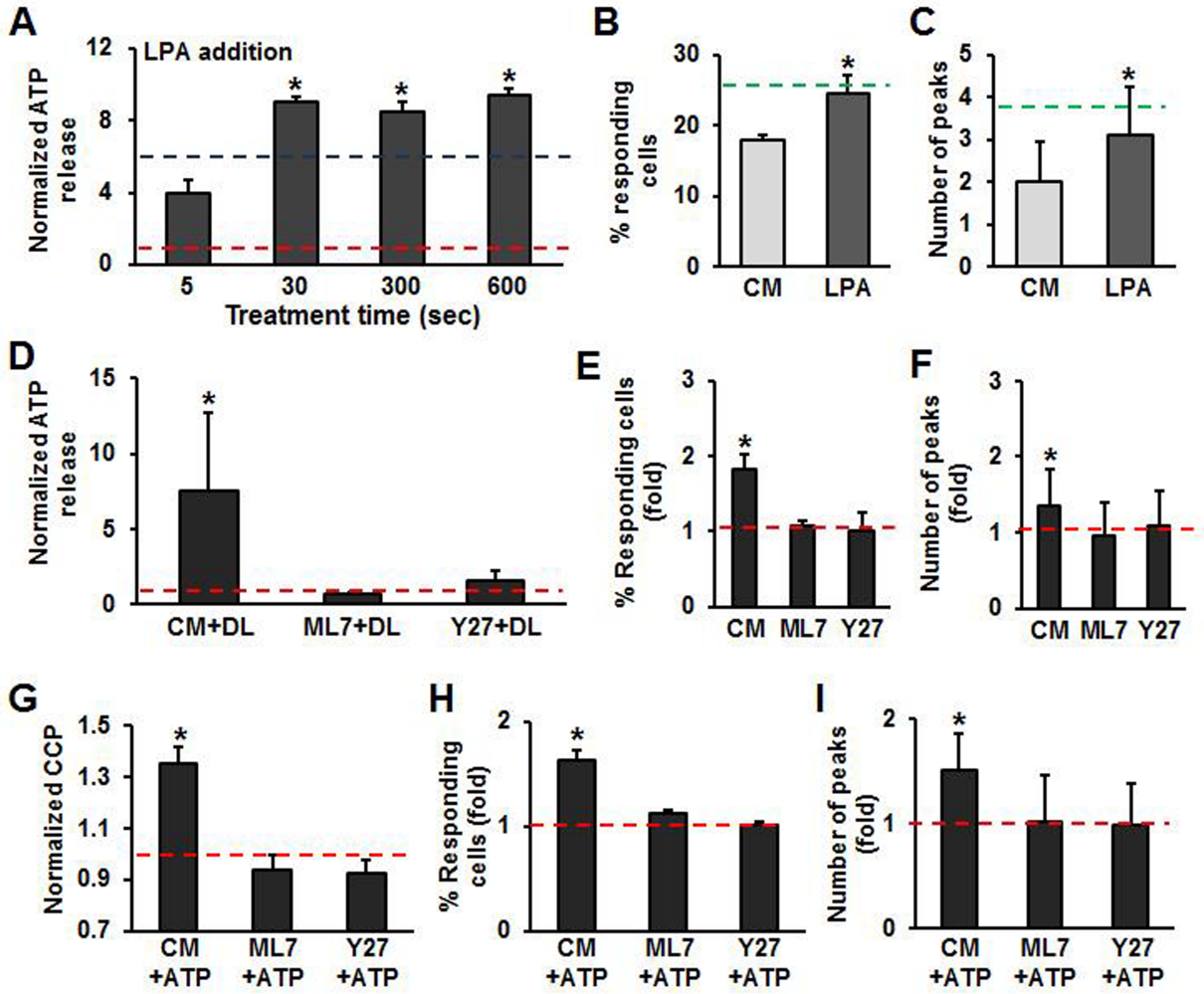
A
LPA addition
Normalized ATP release
12
8
4
0
5
30
300
600
Treatment time (sec)
B
% responding cells
30
20
10
0
CM
LPA
C
Number of peaks
5
4
3
2
1
0
CM
LPA
D
Normalized ATP release
15
10
5
0
CM+DL
ML7+DL
Y27+DL
E
% Responding cells (fold)
3
2
1
0
CM
ML7
Y27
F
Number of peaks (fold)
3
2
1
0
CM
ML7
Y27
G
Normalized CCP
1.5
1.3
1.1
0.9
0.7
CM +ATP
ML7 +ATP
Y27 +ATP
H
% Responding cells (fold)
2
1
0
CM +ATP
ML7 +ATP
Y27 +ATP
I
Number of peaks (fold)
2
1
0
CM +ATP
ML7 +ATP
Y27 +ATP

Figure 4

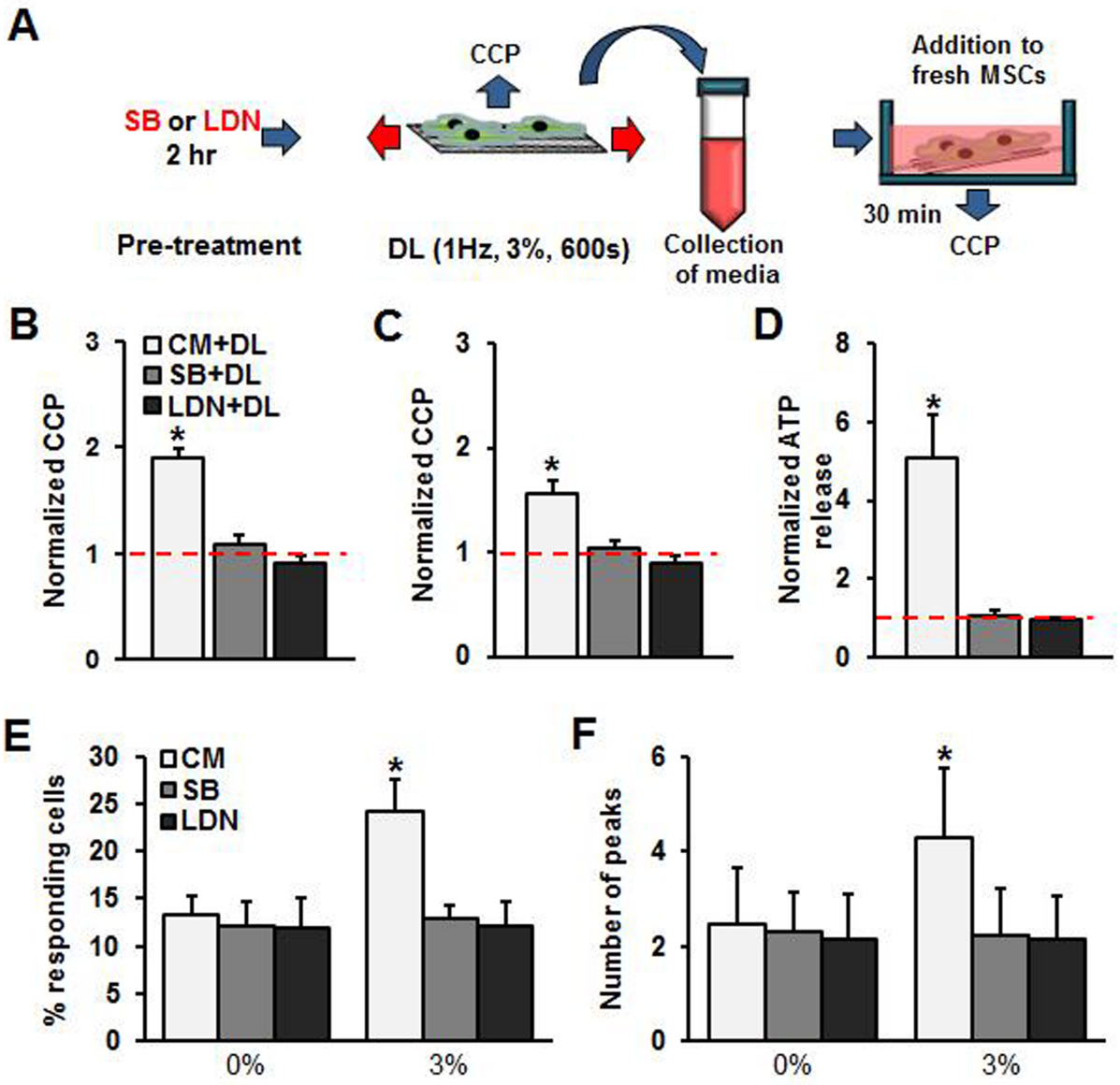
A
SB or LDN
2 hr
Pre-treatment
CCP
DL (1Hz, 3%, 600s)
Collection
of media
Addition to
fresh MSCs
30 min
CCP
B
CM+DL
SB+DL
LDN+DL
Normalized CCP
C
Normalized CCP
D
Normalized ATP
release
E
CM
SB
LDN
% responding cells
0%
3%
F
Number of peaks
0%
3%

Figure 5

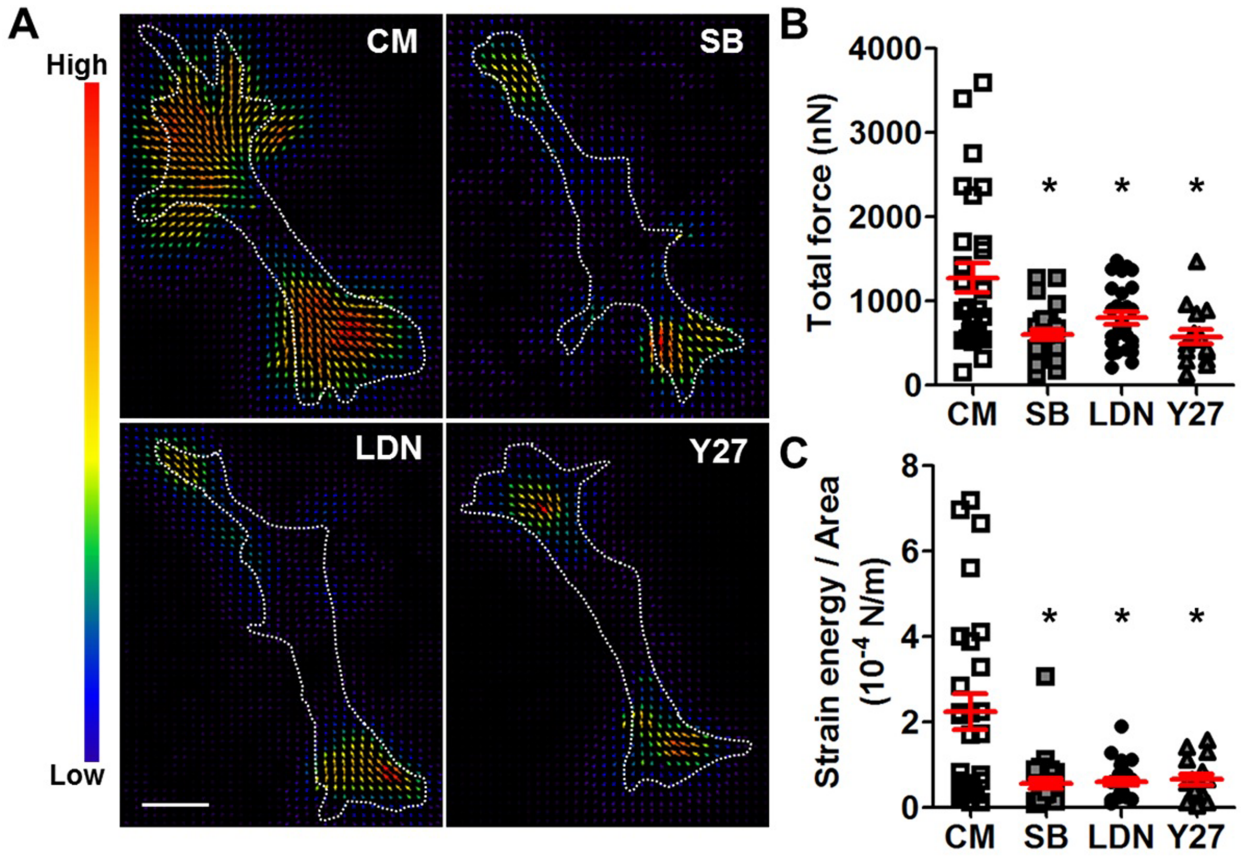
A
High
Low
CM
SB
LDN
Y27
B
Total force (nN)
4000
3000
2000
1000
0
CM
SB
LDN
Y27
C
Strain energy / Area
(10^{-4} N/m)
8
6
4
2
0
CM
SB
LDN
Y27

Figure 6

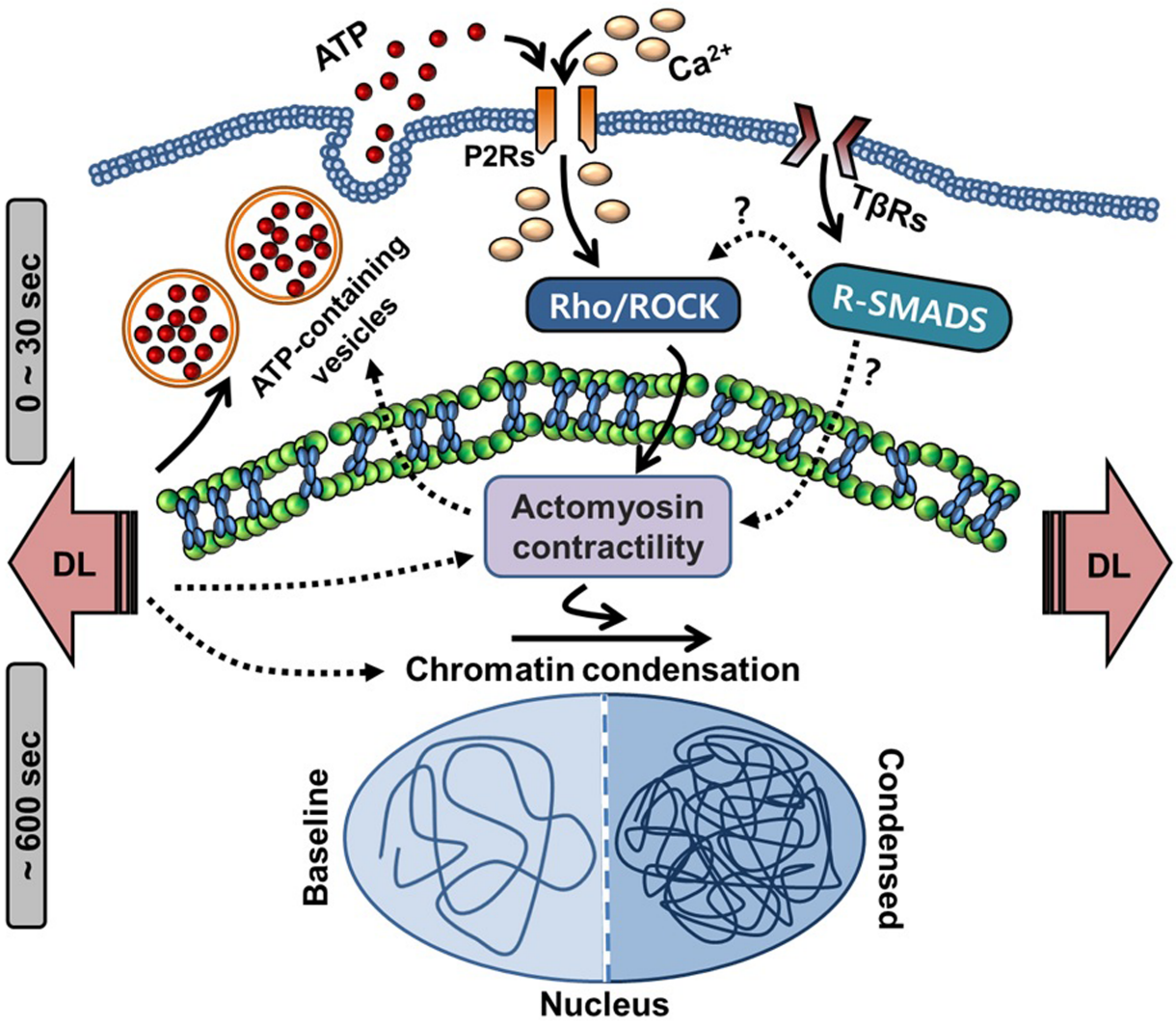
ATP
Ca2+
P2Rs
TβRs
?
Rho/ROCK
R-SMADS
?
ATP-containing vesicles
0 ~ 30 sec
DL
Actomyosin contractility
DL
Chromatin condensation
~ 600 sec
Baseline
Condensed
Nucleus

Figure 7

Supplementary Information for:

Mechanically Induced Chromatin Condensation Requires Cellular Contractility in Mesenchymal Stem Cells

Su-Jin Heo[1,2], Woojin M. Han[2], Spencer E. Szczesny[1,3], Brian D. Cosgrove[1,2,3], Dawn M. Elliott[4], David A. Lee[6], Randall L. Duncan[4,5], and Robert L. Mauck[1,2,3]*

[1]McKay Orthopaedic Research Laboratory, Department of Orthopaedic Surgery, Perelman School of Medicine, University of Pennsylvania, Philadelphia, PA, USA

[2]Department of Bioengineering, School of Engineering and Applied Science, University of Pennsylvania, Philadelphia, PA, USA

[3]Translational Musculoskeletal Research Center, Philadelphia VA Medical Center, Philadelphia, PA, USA

[4]Department of Biomedical Engineering, University of Delaware, Newark, DE, USA

[5]Department of Biological Sciences, University of Delaware, Newark, DE, USA

[6]Institute of Bioengineering, School of Engineering and Materials Science, Queen Mary University of London, London, UK

***Address for Correspondence**:
Robert L. Mauck, Ph.D.
Mary Black Ralston Professor of Orthopaedic Surgery
Professor of Bioengineering

McKay Orthopaedic Research Laboratory
Department of Orthopaedic Surgery
Perelman School of Medicine
University of Pennsylvania
36th Street and Hamilton Walk
Philadelphia, PA 19104
Phone: (215) 898-3294
Fax: (215) 573-2133
Email: lemauck@mail.med.upenn.edu

Supplemental Figures and Legends

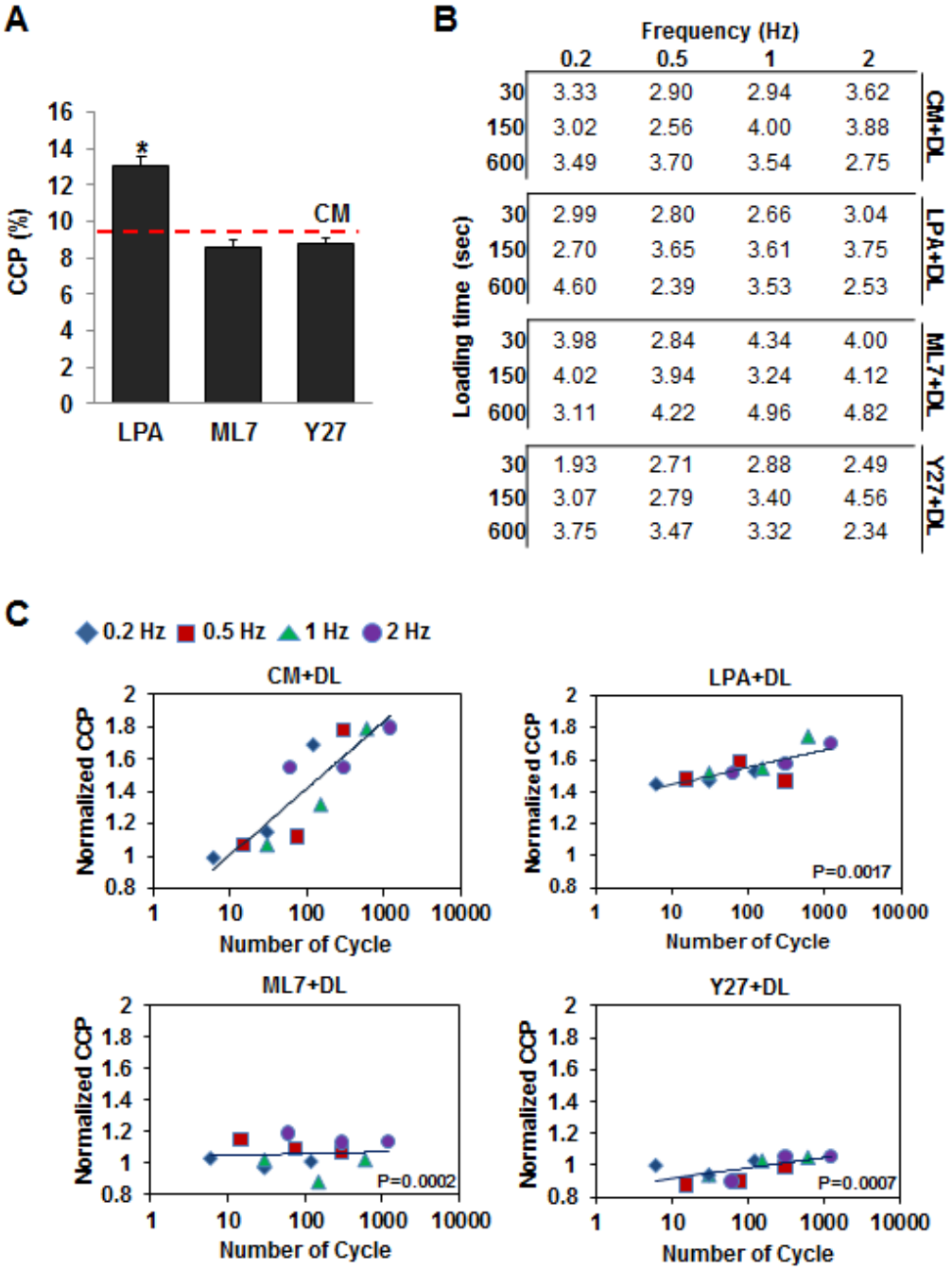

sFigure 1. (A) Baseline CCP values with pre-treatment with LPA, ML7, or Y27 (red line: CM conditions, n = ~ 55 cells per condition per time point, from 3 replicate studies, *: $p<0.05$ vs. CM without DL, mean ± SEM]. (B) Standard deviations for each value provided in figure 1B. (C) Line plots showing the correlation between the number cycles of DL and CCP values with/without agonists and antagonists of contractility. Cells were fixed immediately after the final loading cycle (p values indicate comparisons between the slope of the response in experimental groups to the slope of CM+DL group via F-test, Bonferroni adjusted p value)

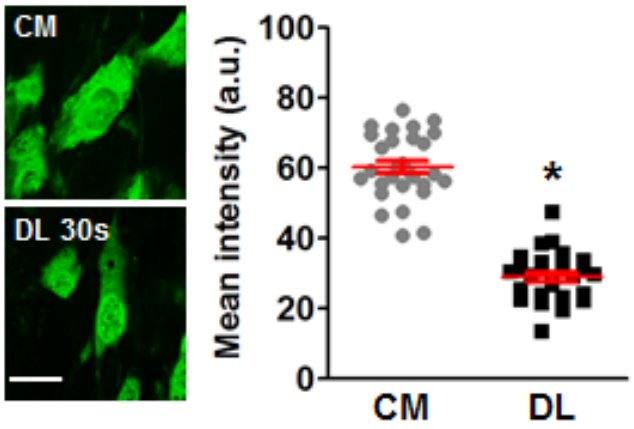

sFigure 2. Quinacrine dihydrochloride staining of ATP-filled vesicles in MSCs before/after the application of DL (1 Hz, 3%, 30 sec, left) and quantification (right, n = ~25, *: p = 0.05, mean ± SEM, scale bar = 20 μm).

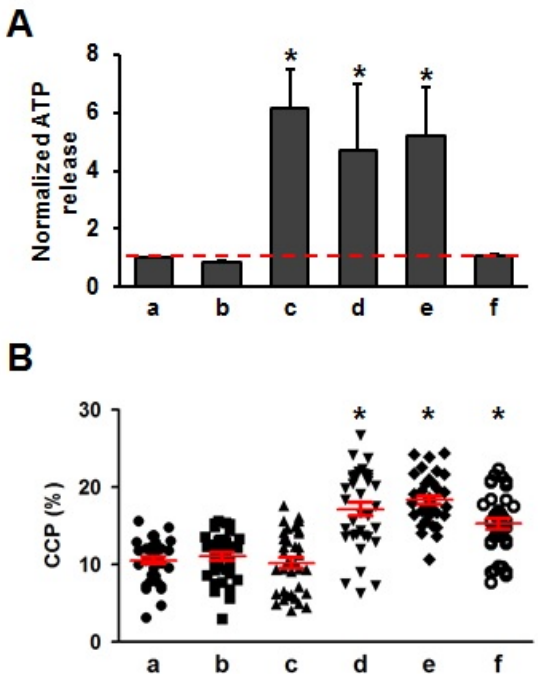

sFigure 3. (A) ATP concentration in conditioned media (normalized to ATP concentration in CM conditions: 65 nM, red line, mean ± SD) and (B) CCP values under various conditions [a: CM media for 600s without DL, b: CM media for 30 sec followed by switching to new fresh media up to 600 sec without DL, c: DL condition (0.2 Hz, 3%, 30 sec), d: DL condition (0.2 Hz, 3%, 600 sec), e: DL condition (0.2 Hz, 3%, 30 sec) followed by free swelling up to 600 sec, f: DL condition (0.2 Hz, 3%, 30 sec) followed by free swelling up to additional 600 sec in fresh media, n = 3 from 3 biological replicates for (A), n = ~35 (B), *: $p<0.05$ vs. a, mean ± SEM].

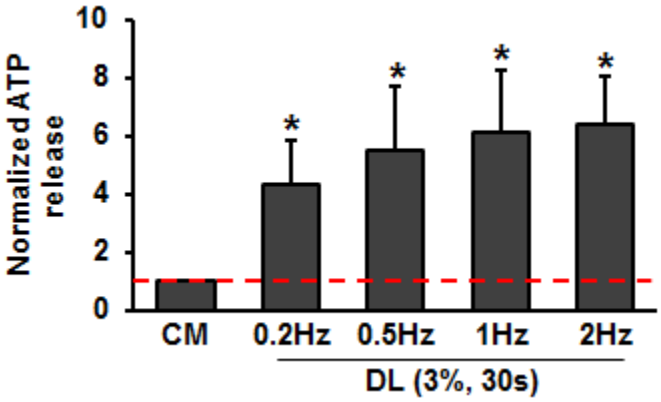

sFigure 4. ATP release in response to DL applied at various frequencies (0.2 Hz ~ 2 Hz, normalized to ATP concentration in CM conditions in red, n = 3 from 3 biological replicates, *: $p<0.05$ vs CM conditions, mean ± SD).

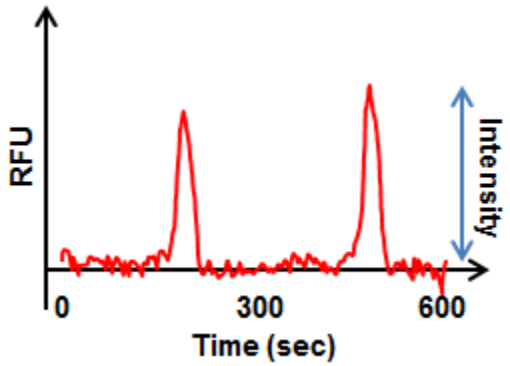

sFigure 5. A representative $[Ca^{2+}]_i$ oscillation curve for MSCs.

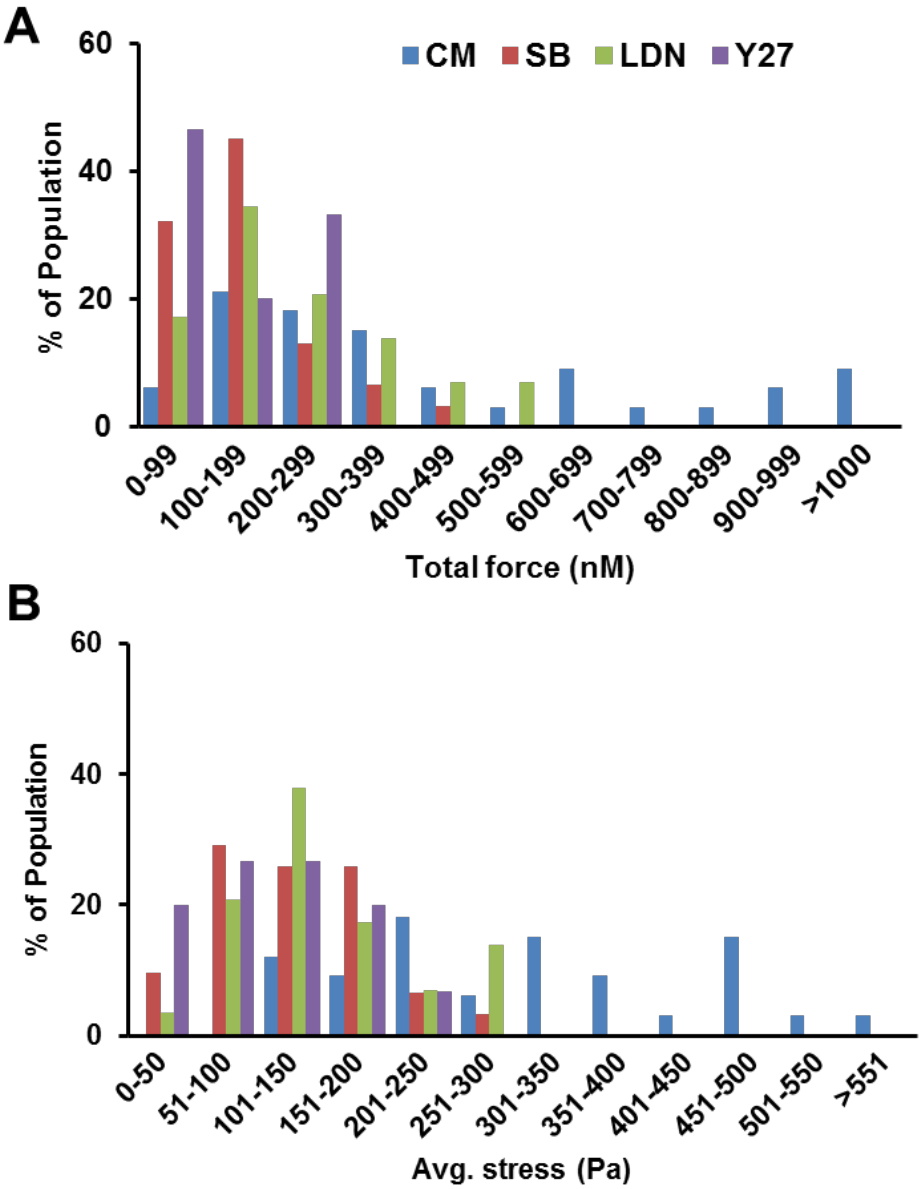

sFigure 6. Population distribution of traction force (a) and average traction stress (b) with/without the addition of SB, LDN or Y27.

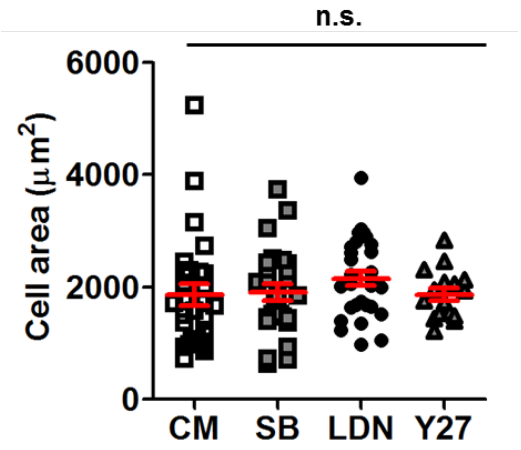

sFigure 7. Quantification of cell area with pharmacological inhibition (n=16~31 cells per group, mean ± SEM).

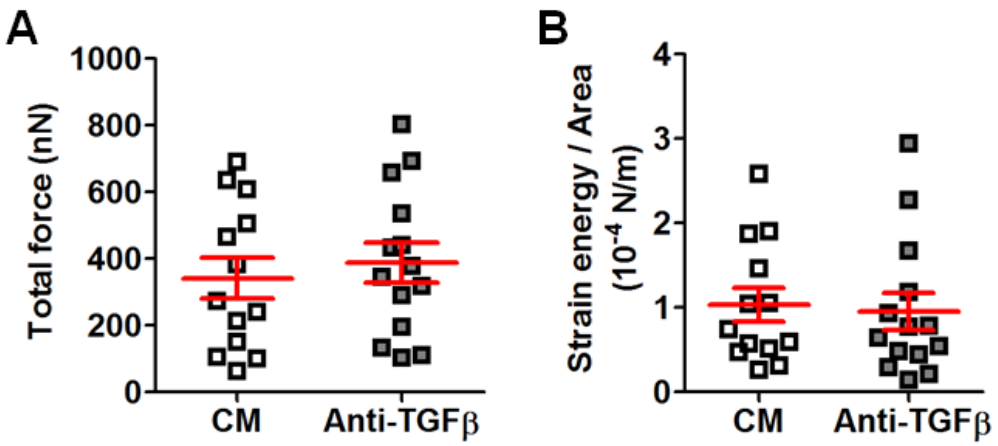

sFigure 8. (A) Quantification of total force per cell (nN) and (B) the ratio of strain energy per cell spread area with treatment with TGF-β neutralizing antibody (Anti-TGFβ, mean ± SEM, n=13~14 cells per group, mean ± SEM).